PNAS RESEARCH ARTICLE | PLANT BIOLOGY

Paired *Medicago* receptors mediate broad-spectrum resistance to nodulation by *Sinorhizobium meliloti* carrying a species-specific gene

Jinge Liu[a,1], Ting Wang[b,1], Qiulin Qin[a], Xiaocheng Yu[a], Shengming Yang[c], Randy D. Dinkins[d], Anett Kuczmog[e], Péter Putnoky[e], Artur Muszyński[f], Joel S. Griffitts[g], Attila Kereszt[b,2], and Hongyan Zhu[a,2]

Edited by Sharon Long, Stanford University, Stanford, CA; received August 27, 2022; accepted November 9, 2022

Plants have evolved the ability to distinguish between symbiotic and pathogenic microbial signals. However, potentially cooperative plant–microbe interactions often abort due to incompatible signaling. The *Nodulation Specificity 1* (*NS1*) locus in the legume *Medicago truncatula* blocks tissue invasion and root nodule induction by many strains of the nitrogen-fixing symbiont *Sinorhizobium meliloti*. Controlling this strain-specific nodulation blockade are two genes at the *NS1* locus, designated *NS1a* and *NS1b*, which encode malectin-like leucine-rich repeat receptor kinases. Expression of *NS1a* and *NS1b* is induced upon inoculation by both compatible and incompatible *Sinorhizobium* strains and is dependent on host perception of bacterial nodulation (Nod) factors. Both presence/absence and sequence polymorphisms of the paired receptors contribute to the evolution and functional diversification of the *NS1* locus. A bacterial gene, designated *rns1*, is required for activation of *NS1*-mediated nodulation restriction. *rns1* encodes a type I-secreted protein and is present in approximately 50% of the nearly 250 sequenced *S. meliloti* strains but not found in over 60 sequenced strains from the closely related species *Sinorhizobium medicae*. *S. meliloti* strains lacking functional *rns1* are able to evade *NS1*-mediated nodulation blockade.

Medicago | nodulation | symbiosis | specificity | receptors

Significance

Legumes can supply their own nitrogen needs through forming a nitrogen-fixing root nodule symbiosis with rhizobia. However, this symbiosis shows a high level of specificity, such that nodulation capacity and nitrogen fixation effectiveness vary enormously between different plant–bacteria interactions. Understanding the plant and bacterial genes that regulate this specificity will facilitate genetic manipulation of the symbiotic partnership to boost its potential for sustainable agriculture. We report the identification of a pair of receptors in the legume *Medicago truncatula* that confer resistance to nodulation by a wide spectrum of *Sinorhizobium meliloti* strains. We also cloned a bacterial gene that is required for activation of this receptor-mediated nodulation restriction. Our discovery reveals a previously undescribed mechanism regulating specificity in host–bacterial symbiosis.

Plants encounter a wide variety of pathogenic and symbiotic microbes in their habitats. Interactions with these microbes are mediated by cell-surface or intracellular receptors that perceive microbial signals to trigger immunity or symbiosis signaling (1–3). Despite their unique features, pathogens and beneficial symbionts present several common microbe-associated molecular patterns and utilize similar tactics to facilitate their infection of the host, thereby requiring host plants to distinguish between them based on species- or strain-specific signals (4–10). However, this level of surveillance is complicated by the fast-evolving nature of such signals and cognate perception mechanisms (11, 12). Consequently, potentially mutualistic interactions often terminate due to a lack of genetic and molecular adaptations between the interacting partners (11, 13).

In the legume–rhizobial symbiosis, bacteria induce the formation of a specialized organ known as the root nodule. The bacteria infect the nodule cells and subsequently differentiate into bacteroids that are capable of nitrogen fixation. In most legumes, rhizobial infection and nodule organogenesis require host recognition of rhizobium-secreted lipochitooligosaccharides known as nodulation (Nod) factors (14). Nod factors dictate the host range of rhizobia, thus functioning as both specificity factors and master-regulatory inputs (9, 15–18). While Nod factor perception is often sufficient for nodule primordium formation, bacterial infection is also modulated by host perception of other rhizobial signals, including secreted effector proteins, microbe-associated molecular patterns, and cell-surface molecules (19–21). Perception of these secondary bacterial signals can trigger or suppress host immunity responses, leading to restriction or promotion of infection depending on host genetic background (21–23). In certain instances, rhizobial-secreted effector proteins can induce root nodule symbiosis in the absence of Nod factor production or recognition (24, 25). Under all these scenarios, symbiosis development requires the bacteria to be able to evade or manipulate host immune responses (3).

Several dominant genes have been cloned in soybeans that confer resistance to rhizobial infection in a strain-specific manner (22, 26, 27). Such genes encode nucleotide-binding leucine-rich repeat immune receptors or defense-response proteins that recognize rhizobial effectors delivered into the plant cell through the type III secretion system, resembling "gene-for-gene" resistance against bacterial pathogens (23, 28). These examples illustrated an important role of effector-triggered immunity in regulation of symbiosis specificity. However, in the *Medicago*–*Sinorhizobium* symbiosis, the bacterial symbionts generally do

Author contributions: J.L., T.W., A.Kereszt, and H.Z. designed research; J.L., T.W., Q.Q., X.Y., S.Y., A.Kuczmog, A.M., and A.Kereszt performed research; S.Y., R.D.D., P.P., A.M., and J.S.G. contributed new reagents/analytic tools; J.L., T.W., Q.Q., X.Y., A.Kereszt, and H.Z. analyzed data; and J.L., A.Kereszt, and H.Z. wrote the paper.

The authors declare no competing interest.

This article is a PNAS Direct Submission.

[1]J.L. and T.W. contributed equally to this work.

[2]To whom correspondence may be addressed. Email: kereszta@gmail.com or hzhu4@uky.edu.

This article contains supporting information online at https://www.pnas.org/lookup/suppl/doi:10.1073/pnas.2214703119/-/DCSupplemental.

Published December 12, 2022.

not possess type III secretion machinery (20), raising the question of how nodulation specificity is regulated in this system. Here, we report the identification of two malectin-like leucine-rich repeat receptor-like kinases at the *Medicago truncatula Nodulation Specificity 1* (*NS1*) locus that function together to confer resistance against many strains of *Sinorhizobium meliloti*. Activation of *NS1*-mediated nodulation restriction requires a species-specific bacterial gene, called *rns1*, which is widely present in *S. meliloti* but absent in the currently sequenced *Sinorhizobium medicae* strains.

Results

***NS1* Locus Confers Resistance to Infection and Nodulation in a Strain-Specific Manner.** We previously identified the *NS1* locus in the *M. truncatula* accession F83005 that restricts nodulation (Nod–) by *S. meliloti* Rm41 (Rm41) (29). When inoculated with Rm41, F83005 formed barely visible nodule primordia devoid of bacteria due to failed initiation or elongation of infection threads, but the plant formed mature nitrogen-fixing nodules (Nod+/Fix+) with other strains such as *S. meliloti* Rm1021 (Rm1021) and *S. medicae* ABS7 (ABS7). The dominant nature of this nodulation-restrictive locus, together with the ability of Rm41 to induce root hair curling and nodule primordium formation, indicates that this incompatibility is not caused by a lack of Nod factor perception or signaling. Moreover, unlike the resistance gene-mediated nodulation restriction in soybeans (22, 26, 27), this specificity is independent of bacterial type III effectors because Rm41 does not possess type III secretion machinery (30).

***NS1* Locus Encodes Two Receptor Kinases, NS1a and NS1b, Both Required for Resistance to Infection and Nodulation by Rm41.** We delimited the *NS1* locus to a small genomic region on chromosome 8, based on linkage mapping in two F2 populations involving three parents, one derived from the cross between F83005 (Nod–) and A20 (Nod+) and another from the cross of F83005 (Nod–) and DZA045 (Nod+). In the reference genome of Jemalong A17 (Nod+/Fix–), this region is ~50 kb in length and annotated as containing a gene (*Medtr8g028110)* that consists of 13 exons and encodes a receptor-like kinase (version Mt 4.0) (31) (Fig. 1*A*). This receptor-like kinase comprises an N-terminal signal peptide, an extracellular malectin-like domain, at least three predicted leucine-rich repeats, a single-pass transmembrane (TM), and an intracellular serine-threonine kinase domain. Notably, adjacent to *Medtr8g028110* is a partial duplication (annotated

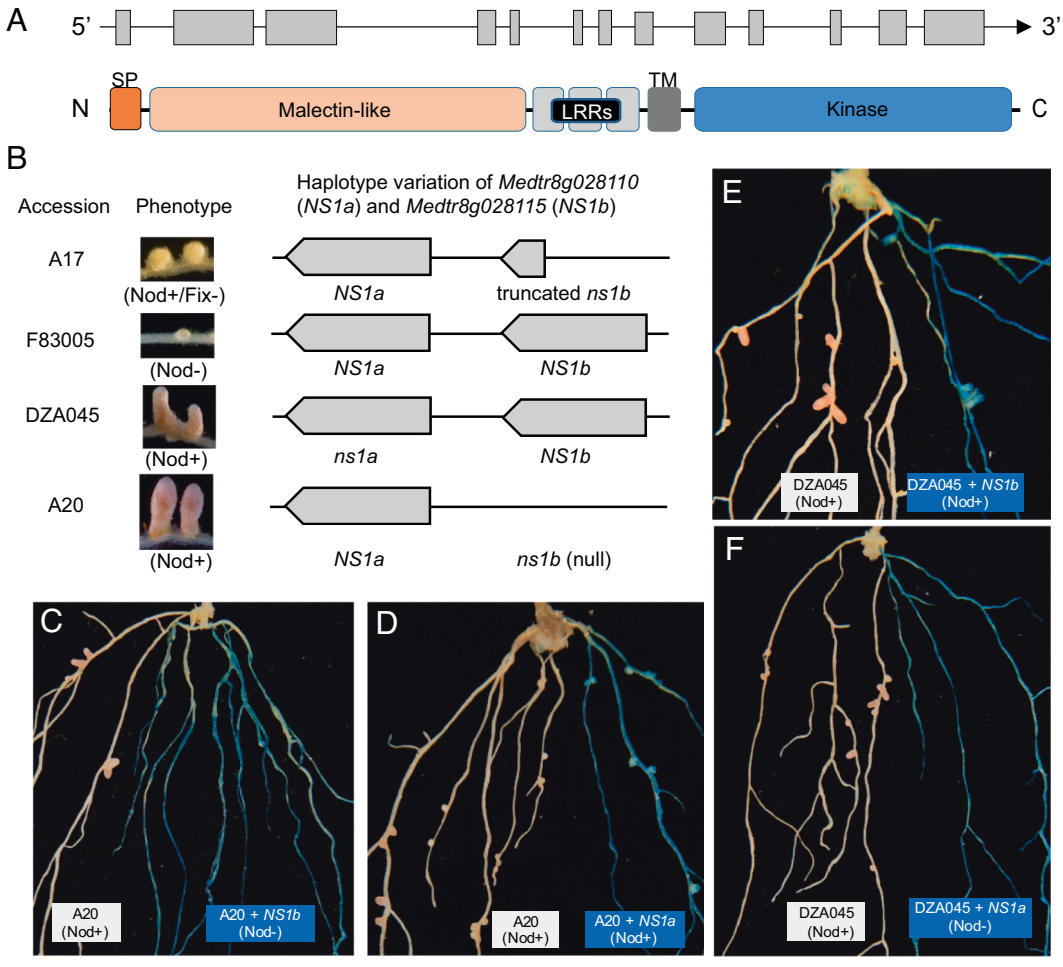

Fig. 1. Positional cloning and functional validation of the candidate genes at the *NS1* locus. (*A*) *Top*: Gene structure of *NS1a and NS1b*. The exons and introns are indicated by boxes and lines, respectively. *Bottom*: Diagram presenting the domain structure of the NS1a and NS1b proteins. SP, signal peptide; LRRs, leucine-rich repeats; TM, transmembrane domain. (*B*) Genomic organization of the candidate genes *NS1a* and *NS1b* in the three mapping parents and the reference genotype Jemalong A17, showing the presence/absence polymorphisms and the dominant/recessive alleles. (*C–F*) Functional validation of the candidate genes by complementation tests. The transgenic hairy roots (blue) were distinguished from wild-type ones (white) by GUS staining. Introduction of *NS1b* (F83005) into A20 led to prevention of nodulation on the transgenic roots (*C*), while the transgenic A20 roots expressing the *NS1a* allele of F83005 retained the Nod+ phenotype (*D*). Conversely, transgenic roots expressing the *NS1b* allele of F83005 in DZA045 failed to convert the Nod+ phenotype to Nod− (*E*), but transfer of *NS1a* of F83005 into DZA045 confers resistance to nodulation by Rm41 (*F*). At least 40 transgenic hairy roots were obtained for each experiment and all showed the same results.

as *Medtr8g028115*) encoding a partial kinase domain (Fig. 1*B*). Sequencing and annotation of the genomic regions surrounding the *NS1* locus of the three parents revealed both presence/absence and sequence-level polymorphisms for the two tandem gene copies (Fig. 1*B* and *SI Appendix*, Figs. S1–S3). In particular, F83005 (Nod–) and DZA045 (Nod+) both possess full-length copies of *Medtr8g028110* and *Medtr8g028115*, while *Medtr8g028115* is missing in the genome of A20 (Nod+). We therefore postulated that *Medtr8g028110* (hereafter referred to as *NS1a*) and *Medtr8g028115* (hereafter referred to as *NS1b*) constitute the functional *NS1* locus in F83005 controlling resistance to infection by Rm41.

We explored the dominant/recessive nature of *NS1a* and *NS1b* in A20 and DZA045 through transgenic complementation (Fig. 1*B*). The absence of an *NS1b* allele in A20 (Nod+) and a lack of nonsynonymous substitutions between the *NS1a* alleles of A20 (Nod+) and F83005 (Nod–) (*SI Appendix*, Fig. S1) suggested that the *NS1b* allele of F83005 (Nod–) prevents nodulation by Rm41. Consistent with this reasoning, transgenic hairy roots of A20 expressing the *NS1b* allele of F83005 (Nod–) showed a Nod– phenotype (Fig. 1*C*), while transgenic roots expressing the *NS1a* allele of F83005 retained the Nod+ phenotype (Fig. 1*D*). Surprisingly however, no nonsynonymous substitutions exist between the *NS1b* alleles of F83005 (Nod–) and DZA045 (Nod+) within the cosegregated region (*SI Appendix*, Fig. S2); accordingly, introduction of the *NS1b* allele of F83005 (Nod–) into DZA045 (Nod+) failed to convert the Nod+ phenotype to Nod– (Fig. 1*E*). However, the *NS1a* alleles are polymorphic between the two parents (*SI Appendix*, Fig. S1), and transfer of *NS1a* of F83005 (Nod–) into DZA045 (Nod+) prevented nodulation by Rm41 (Fig. 1*F*). Based on these experiments, we concluded that *NS1a* and *NS1b* are both required for nodulation restriction in F83005 (Nod–). We further validated this conclusion by CRISPR/Cas9-mediated gene knockouts (*SI Appendix*, Fig. S4). For this purpose, we designed single-guide RNAs (sgRNAs) that targeted either or both of *NS1a* and *NS1b* in F83005 (Nod–). The experiments demonstrated that knockout of either of the two genes led to the formation of mature infected nodules.

Expression of *NS1a* and *NS1b* Is Induced and Dependent on Host Perception of Nod Factors. A search of the *M. truncatula* Gene Expression Atlas (MtExpress V2) for the reference genotype Jemalong A17 (containing only *NS1a*) suggested specific expression of *NS1a* in rhizobium-inoculated roots and nodules (Fig. 2 *A* and *B*) (32–34). In the fully developed nodules, *NS1a* was predominantly expressed in the meristematic and infection zones (Fig. 2*B*) (33, 34). We further analyzed the expression pattern of *NS1a* and *NS1b* by assaying their promoter activity in the transformed roots of F83005 using the *pNS1a/b*::*GUS* reporters. GUS (β-glucuronidase) activity was barely detectable in noninoculated transgenic roots but strongly induced upon inoculation with either incompatible (Rm41) or compatible (ABS7) strains, and such induced expression occurred exclusively in the susceptible zone prone to rhizobial colonization or differentiation zones forming nodule primordia (Fig. 2 *C* and *D* and *SI Appendix*, Fig. S5). We next used the *NS1a* and *NS1b* promoters to drive the expression of a nuclear-localized eYFP reporter enhanced yellow fluorescent protein-nuclear localization signal (eYFP-NLS). This experiment revealed the expression of *pNS1a/b:eYFP-NLS* in both epidermal and cortical cells of the nodule primordium (Fig. 2 *E* and *F* and *SI Appendix*, Fig. S5). These observations suggested that the expression of *NS1a* and *NS1b* is dependent on host perception of Nod factors. Supporting this inference, a *nodC* mutant of Rm41 deficient in Nod–factor biosynthesis failed to induce the *NS1a* and

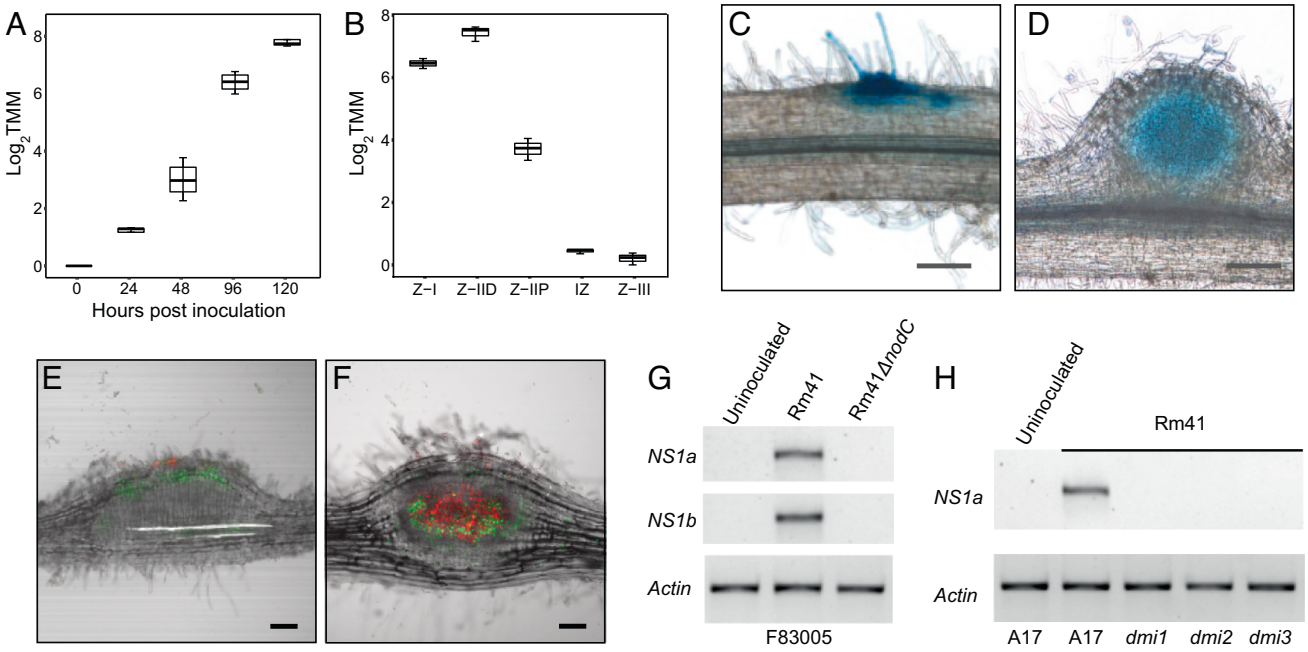

Fig. 2. Expression of *NS1a*. (*A* and *B*) RNA-seq analysis of *NS1a* expression in rhizobium-inoculated roots (*A*) and nodules (*B*) of Jemalong A17. The data from previously published experiments were extracted from the MtExpress V2 database (32–34). Trimmed Mean of M-values-normalized counts were used for analysis. In the boxplots, whiskers represent the minimum/maximum values, the box defines the interquartile range, the centerline represents the median, and box bounds represent the lower and upper quartiles. Z-I, meristematic zone; Z-IID, distal infection zone; Z-IIP, proximal infection zone; Z-III, nitrogen-fixation zone; IZ, interzone between Z-II and Z-III. (*C* and *D*) Expression of *pNS1a*::*GUS* in transgenic hairy roots of F83005 inoculated by Rm41 (*C*) and ABS7 (*D*). GUS staining images of *Agrobacterium rhizogenes*-mediated transformed hairy roots were taken 10 d post inoculation. GUS activity was observed only in susceptible zones or nodules. (Scale bars, 100 μm.) (*E* and *F*) Expression of *pNS1a*::*eYFP-NLS* in transgenic hairy roots inoculated by Rm41 (*E*) and ABS7 (*F*); Confocal microscopic images were captured 10 d post inoculation. Rhizobia were labeled with DsRed. (Scale bars, 100 μm.) (*G* and *H*) RT-PCR analysis of *NS1a* and/or *NS1b* expression in the roots of F83005 inoculated by a *nodC* mutant of Rm41 (*G*) and in the roots of the A17 *dmi1-3* mutants inoculated by wild-type Rm41 (*H*).

NS1b expression in the roots of F83005 (Fig. 2*G*), and the plant mutants defective in Nod factor signaling (i.e., *dmi1*, *dmi2*, and *dmi3*) in the A17 background were also unable to express *NS1a* in the rhizobium-inoculated roots (Fig. 2*H*). Furthermore, *NS1a* expression was absent in the rhizobium-inoculated roots of plant mutants defective in Nod factor perception (i.e., *nfp* and *lyk3*) (33, 35).

NS1a Interacts with NS1b at the Plasma Membrane. We generated a translational fusion of NS1a to an enhanced green fluorescent protein (eGFP) and showed that the protein localized to the plasma membrane based on transient expression in *Nicotiana benthamiana* leaves (Fig. 3*A*). Because of the dependence of both NS1a and NS1b for resistance to infection by Rm41, we tested whether the two receptor-like kinases physically interact with each other. We first performed bimolecular fluorescence complementation (BiFC) assays in *Nicotiana benthamiana* leaves. This experiment suggested that NS1a interacts with a truncated version of NS1b consisting of the extracellular domain (ECD) and TM ($NS1b^{ECD+TM}$) and that NS1a, but not NS1b, self-associates to form homomers; however, they do not interact with Does Not Make Infections 2 (DMI2), an essential signaling component in the nodulation pathway that shares a similar domain structure with NS1a and NS1b (Fig. 3*B*). We further validated the interactions by pull-down assays using DMI2 as a negative control. For the pull-down assay, we expressed the FLAG (DYKDDDDK)- or six histidine (HIS)-tagged ECDs of NS1a and NS1b in insect cells. The insect cell-expressed $NS1a^{ECD}$-HIS and $NS1b^{ECD}$-HIS, but not $DMI2^{ECD}$-HIS, were pulled down by $NS1a^{ECD}$-FLAG (Fig. 3*C*), and $NS1a^{ECD}$-HIS was pulled down by $NS1b^{ECD}$-FLAG (Fig. 3*D*), supporting the results from the BiFC experiments.

Identification of *rns1*, A Rhizobial Gene Required for Activation of *NS1*-Mediated Resistance to Nodulation. To search for the bacterial molecule that activates *NS1*-mediated nodulation restriction, we carried out random mutagenesis of Rm41 using a *Rhizobiaceae* compatible *mariner* transposon (36). This effort led to isolation of three independent insertion mutants in the coding region of BN406_06091 that gained the ability to infect and nodulate F83005 but did not alter the compatible interactions with A20 and DZA045 (Fig. 4 *A* and *B*). The transposon insertion sites were located at the positions 376, 661, and 737 from the start codon. Creating a targeted insertion mutant of this gene using a spectinomycin resistance gene cassette (cloned into the SmaI site at the position 568) further validated its essential role in eliciting *NS1*-mediated nodulation restriction. We thus named this gene *rns1* (required for activation of the NS1 locus) and chose one of the transposon insertion mutants (insertion at the position 376), designated Rm41_*rns1*::Tn, for further experiments.

rns1 is predicted to encode a protein of 449 amino acids, containing at its N terminus five parallel beta-helix (PbH1) repeats (Fig. 4*A*) that are often present in polysaccharide lyases such as pectate lyases and

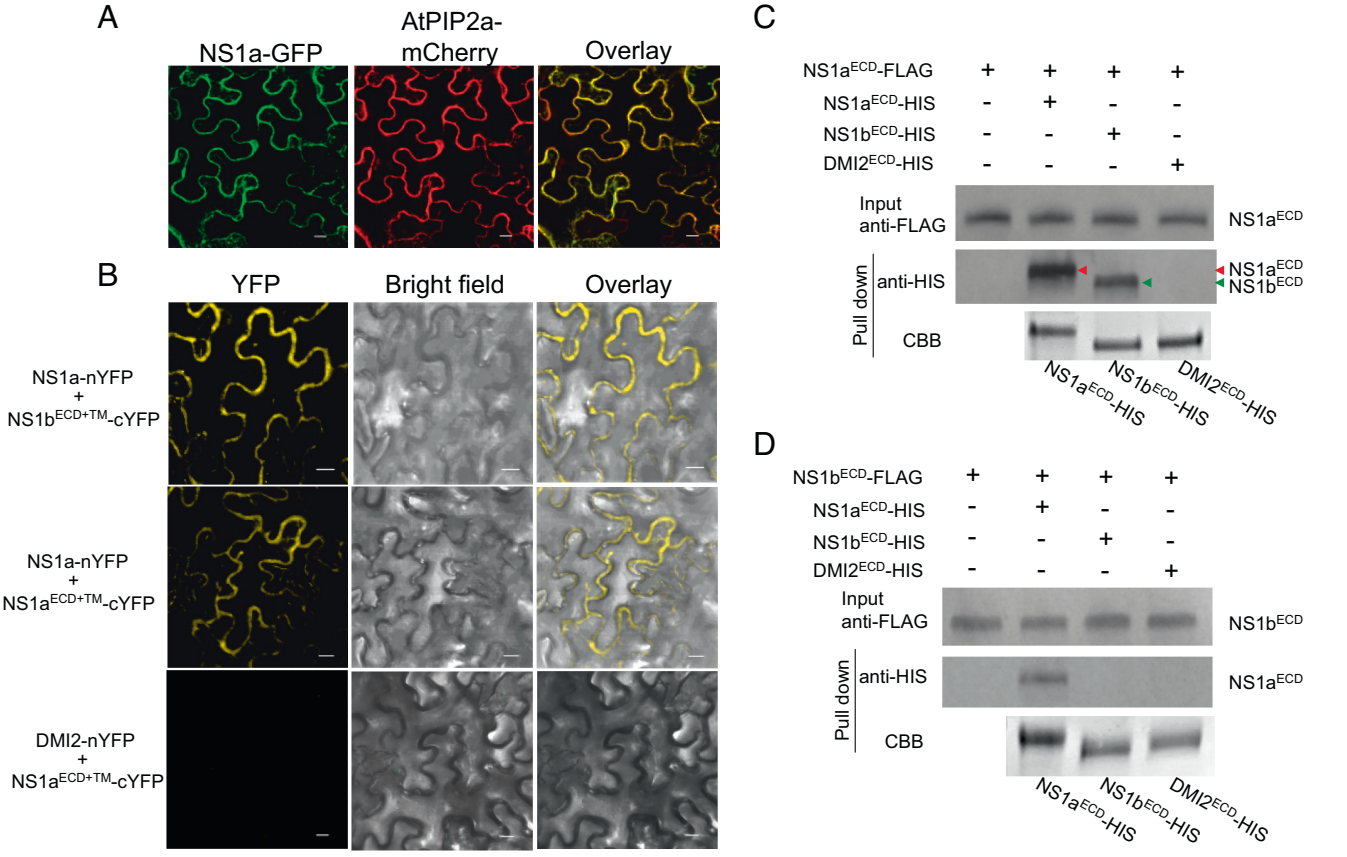

Fig. 3. Interaction of NS1a and NS1b. (*A*) Localization of NS1a in the plasma membrane. NS1a tagged with eGFP at its C terminal was transiently expressed in *N. benthamiana* epidermal cells and analyzed by confocal laser scanning microscopy. The plasma membrane marker AtPIP2a-mCherry was used as a control. (Scale bars, 20 μm.) (*B*) BiFC assays showing interaction of NS1a and $NS1b^{ECD+TM}$ (*Top*), self-association of NS1a and $NS1a^{ECD+TM}$ (*Middle*), and no detectable interaction between DMI2 and $NS1a^{ECD+TM}$ (*Bottom*) in *N. benthamiana* epidermal cells. $NS1a^{ECD+TM}$ = $NS1a^{1–541}$ and $NS1b^{ECD+TM}$ = $NS1a^{1–539}$ (*SI Appendix*, Fig. S3). (Scale bars, 20 μm.) (*C*) Pull-down assays showing interaction of $NS1a^{ECD}$-FLAG and $NS1b^{ECD}$-HIS and self-association of $NS1a^{ECD}$-FLAG and $NS1a^{ECD}$-HIS using NS1a-FLAG as a bait. (*D*) Pull-down assays showing interaction of $NS1a^{ECD}$-HIS and $NS1b^{ECD}$-FLAG using $NS1b^{ECD}$-FLAG as a bait. Coomassie Brilliant Blue (CBB) staining of $NS1a^{ECD}$-HIS, $NS1b^{ECD}$-HIS and $DMI2^{ECD}$-HIS are shown as loading controls. $NS1a^{ECD}$ = $NS1a^{29–514}$, $NS1b^{ECD}$ = $NS1b^{29–512}$ and $DMI2^{ECD}$ = $DMI2^{30–521}$; The ECD coding sequences were codon-optimized for insect cell expression and engineered with an N-terminal gp67 secretion SP.

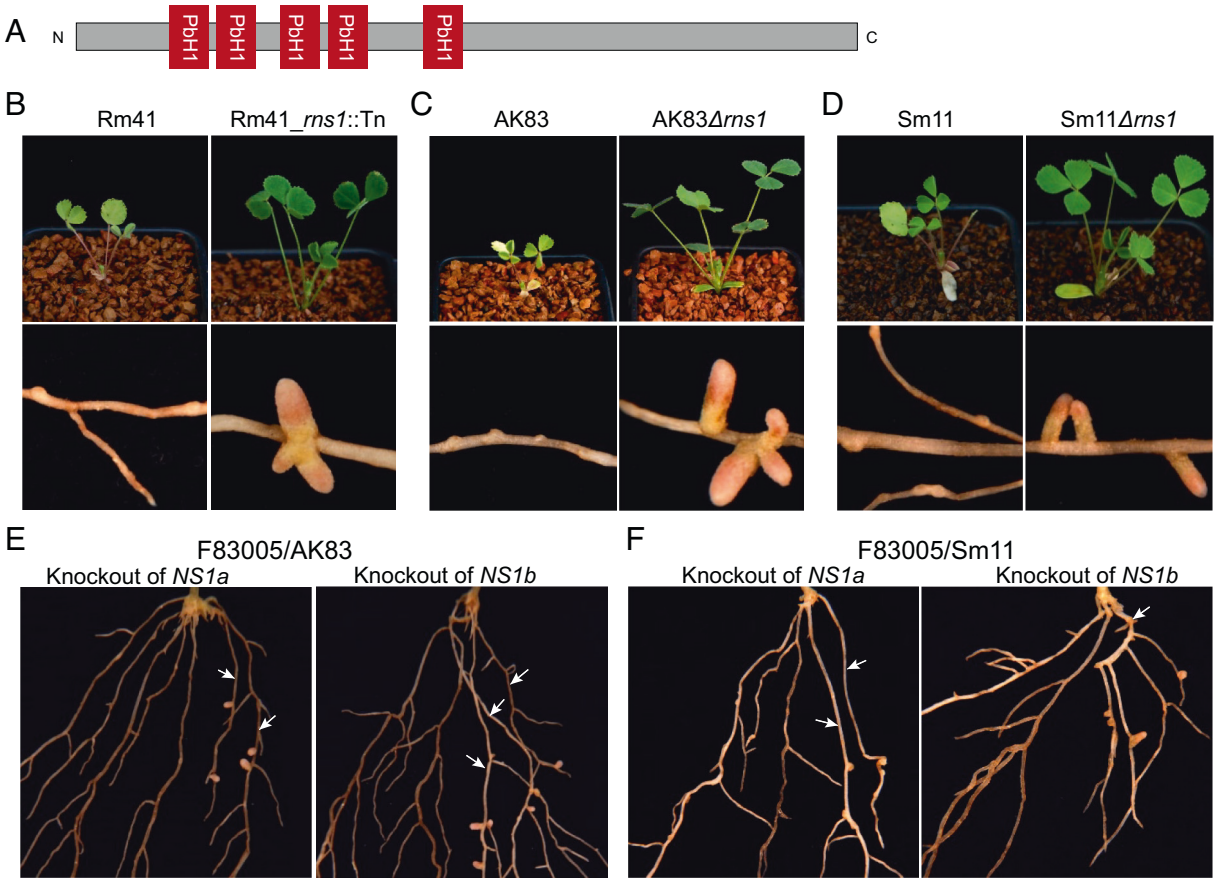

Fig. 4. Functional validation of *rns1*. (*A*) Domain structure of Rns1, consisting of five predicted parallel beta-helix (PbH1) repeats at its N terminus. (*B–D*) Loss-of-function mutation of *rns1* in the F83005-incompatible strains Rm41 (*B*), AK83 (*C*), and Sm11 (*D*) produced a Nod+ phenotype on F83005. (*E* and *F*) CRISPR/Cas9-mediated knockout of *NS1a* or *NS1b* in F83005 enables nodulation of the knockout roots with AK83 (*E*) and Sm11 (*F*). The arrows indicate the knockout roots forming nitrogen-fixing pink nodules. Plants and root nodules were photographed 3 wk post inoculation.

exopolysaccharide (EPS) glycanases (37, 38). Notably, *rns1* is located in an ~55-kb strain-specific gene cluster on the megaplasmid pSymB that is present in approximately 50% of the nearly 250 sequenced *S. meliloti* strains (e.g., AK83 and Sm11 described below) but missing in many others including the reference strain Rm1021 (*SI Appendix*, Table S1) (39). However, Basic Local Alignment Search Tool (BLAST) searches did not identify the presence of *rns1* in over 60 sequenced *S. medicae* genomes. Most genes in this cluster are predicted to be involved in polysaccharide biosynthesis or transport, and the presence/absence of *rns1* is associated with the dynamic architecture of this gene cluster. We further characterized the strains AK83 and Sm11 that carry this gene cluster along with a functional *rns1* gene and are incompatible with F83005. We demonstrated that the incompatibility of AK83 and Sm11 with F83005 is also conditioned by the *NS1* locus and dependent on the *rns1* gene. Deletion of *rns1* in AK83 (AK83Δ*rns1*) and Sm11 (Sm11Δ*rns1*) (Fig. 4 *C* and *D*) or knockout of either *NS1a* or *NS1b* in F83005 (Fig. 4 *E* and *F*) converted the incompatible interactions into compatible, and the bacterial mutants remained compatible with A20 and DZA045 (*SI Appendix*, Fig. S6). We noted that AK83 was previously reported to be Fix- on certain *Medicago* genotypes, which was hypothesized to be due to absence of genes for microaerophilic growth (40). However, AK83 forms Fix+ nodules with A20 and DZA045, and it is striking that it regains Fix+ phenotype with F83005 when the *rns1* gene is deleted.

Rns1 Activates *NS1*-Mediated Nodulation Restriction When Expressed in Compatible Strains Rm1021 and ABS7. In view of the coexistence of *rns1* with the strain-specific gene cluster, we wondered whether other linked genes in the cluster may also be required for *NS1*-mediated nodulation restriction. We addressed this question by transforming the F83005-compatible strains Rm1021 and ABS7 lacking the *rns1* gene cluster with the broad host-range vector pHC60 expressing *rns1* under control of its native promoter (pRNS1). The pRNS1 plasmid was able to complement Rm41_*rns1*::Tn back to the Rm41 wild-type phenotype (Fig. 5*A*). Our experiments showed that the two transformed strains Rm1021/pRNS1 and ABS7/pRNS1 became incompatible with F83005 while remaining compatible with A20 and DZA045 (Fig. 5 *B* and *C* and *SI Appendix*, Fig. S7). We further explored the association of *rns1* with *NS1*-mediated incompatibility by screening 55 *S. meliloti* and *S. medicae* strains for their nodulation capability on F83005. The experiment revealed that strains carrying this gene cluster along with the *rns1* gene are incompatible with F83005, while strains lacking *rns1* or carrying insertion/deletion mutations in *rns1* are compatible (*SI Appendix*, Table S2 and Fig. S8).

Rns1 Is a Type I-Secreted Protein. Rns1 shares a similar domain structure with PlyA and PlyB, two *Rhizobium leguminosarum* extracellular glycanases that are secreted via a type I secretion system (T1SS) (38). To test whether Rns1 is also a secreted protein, we transformed Rm41_*rns1*::Tn with a pHC60 plasmid expressing both an Hemagglutinin (HA)-tagged Rns1 and a GFP protein (pRNS1-HA/GFP). The transformed strain showed a similar nodulation phenotype as wild-type Rm41, demonstrating that fusion of the HA tag to the C terminus of Rns1 maintained its

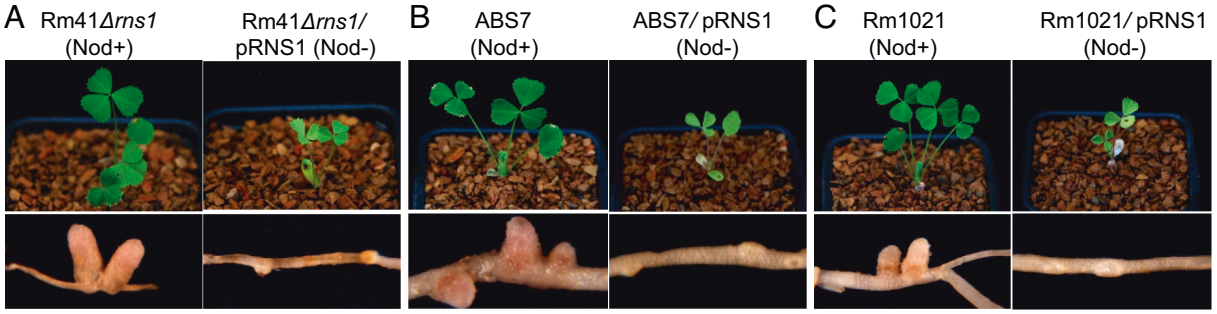

Fig. 5. Rns1 elicits a Nod− phenotype on the roots of F83005 when expressed in the compatible strains ABS7 and Rm1021. (*A*) pRNS1 complemented Rm41Δ*rns1* back to the Rm41 wild-type phenotype (Nod−). (*B* and *C*) Introducing pRNS1 into ABS7 (*B*) and Rm1021 (*C*) resulted in a Nod− phenotype. Plants and root nodules were photographed 3 wk post inoculation. Experiments were repeated three times with similar results.

function (*SI Appendix*, Fig. S9*A*). We were able to detect the presence of HA-tagged Rns1 (but not GFP) in the culture supernatant of Rm41_*rns1*::Tn transformed with pRNS1-HA/GFP, indicating that Rns1 is a secreted protein (Fig. 6). To examine whether the Rns1 secretion is dependent on T1SS, we created an Rm41 mutant, designated Rm41Δ*tolC*, in which the *tolC* gene (BN406_01245) that encodes an outer membrane protein essential for assembling a functional T1SS was deleted. Rm41Δ*tolC* was defective in nodulation with Rm41-compatible plant genotypes, forming only a reduced number of Fix- nodules, and unable to nodulate F83005 (*SI Appendix*, Fig. S9*B*), presumably because the mutant affects EPS biosynthesis and secretion, which is essential for symbiosis development in *Medicago* (41). Rns1 was not detectable in the culture supernatant of Rm41Δ*tolC* transformed with pRNS1-HA/GFP (Fig. 6), suggesting that Rns1 secretion is mediated by T1SS. Despite being a secreted protein, we were not able to detect physical interactions between Rns1 and NS1a/b proteins.

Discussion

Monitoring microbial signals by host receptors plays a central role in regulating the outcomes of plant–microbe interactions. We have demonstrated that *NS1*-mediated resistance to nodulation in *M. truncatula* is conferred by a pair of receptor-like kinases, NS1a and NS1b, which function together to discriminate against *S. meliloti* strains carrying a species-specific *rns1* gene. The *NS1* locus appears to be specific to the *Medicago* lineage because the gene content flanking the *NS1* locus is highly conserved in non-*Medicago* legumes, but *NS1a* and *NS1b* orthologs appear to be constrained to the *Medicago* genus, appearing in the genomes of *M. truncatula*, *Medicago sativa* and *Medicago italica* (*SI Appendix*, Table S3). The presence of both *NS1a* and *NS1b* alleles is rare among *M. truncatula* accessions, suggesting a selection against the distribution of this resistance locus in natural populations because it precludes nodulation with a large number of *S. meliloti* strains. The significance of the induced expression of *NS1a* and *NS1b* by Nod factor perception is not clear, given that both genes are dispensable for nodulation with compatible strains. The expression of these genes may enhance nodulation capacity in compatible interactions, which was not perceived by this study.

The *rns1* gene is widespread in *S. meliloti* but presents numerous loss-of-function variants, suggesting coevolutionary interactions between host and symbionts to promote symbiosis development. However, we did not detect physical interaction of Rns1 with the NS1a/b receptors, suggesting that Rns1 is not a direct ligand recognized by the receptors or there may be other bacterial proteins involved in the recognition process. The presence of the *rns1* gene cluster could affect structural features of cell-surface polysaccharides that facilitate adaptation of the bacterium to its specific niche. Since NS1a and NS1b both contain a putative carbohydrate-binding domain of malectin, we envisaged that NS1a and NS1b receptors might mediate perception of rhizobial surface polysaccharides or their metabolites that are known to play roles in modulating host–bacterial interactions (21, 42–44). We actually generated a series of Rm41 mutants that are defective in the production of capsular polysaccharide (KPS), EPS, or lipopolysaccharide (LPS) and assayed their nodulation phenotypes with F83005, A20, and DZA045. These experiments demonstrated

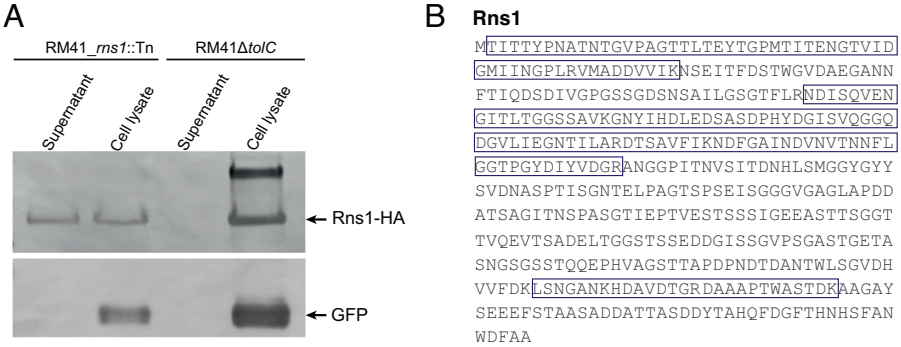

Fig. 6. Rns1 is a type I-secreted protein. (*A*) The HA-tagged Rns1 was detected in the culture supernatant of the Rm41_*rns1*::Tn strain transformed with pRNS1-HA/GFP, but not detected in the culture supernatant of Rm41Δ*tolC* transformed with the same plasmid. The nonsecreted GFP protein was used as a negative control. It is noteworthy that the band size of Rns1-HA in the immunoblot was significantly larger than the predicted size, and in the *tolC* mutant, there existed an additional larger band. These observations are probably due to posttranslational modification of the Rns1 protein, which is further complicated by the disruption of the T1SS machinery. (*B*) The putative Rns1-HA band from the supernatant was subjected to in gel digestion with trypsin followed by LC–MS/MS analysis. This analysis identified 45 peptide fragments from Rns1, covering ~39% of the protein (boxed).

that the *rkp-1*, *rkpK*, and *rkpM* mutants defective in KPS production and the *lpsL*, *lpsB*, and *lpsC* mutants impaired in LPS core and O-antigen biosynthesis all behaved similarly to the wild-type Rm41, suggesting that KPS and LPS are neither essential for nodulation nor bacterial determinants of symbiosis compatibility in the tested plant genotypes. In contrast, the *exoB* (AK631) and *exoY* mutants deficient in EPS production failed to nodulate all the three genotypes, indicating that EPS biosynthesis is indispensable for establishing a symbiosis with the compatible plant genotypes. However, whether recognition specificity associated with the *NS1* locus involves EPS remains elusive. It is conceivable that EPS are required for nodulation but the same EPS or their metabolic derivatives may also serve as the signals to trigger immune responses in the presence of the *NS1* locus (45); under this scenario, disruption of EPS production renders a rhizobium incompatible with all the three genotypes. Further research is needed to identify other bacterial genes involved in the specificity determination, address the biochemical function of Rns1, identify the ligand of the receptors, and characterize the downstream signaling, which will provide new insights into the molecular mechanisms that regulate specificity in plant–microbe interactions.

Materials and Methods

Plant Material and Nodulation Assay. *M. truncatula* accessions used in this study included Jemalong A17, A20, F83005.5 (F83005), and DZA045.5 (DZA045). Seeds were treated with concentrated sulfuric acid and geminated on wet filter papers in the dark for 2 d. Seeds with emerging radicles were transferred to plastic pots filled with sterilized vermiculite (PVP Industries, Inc.) and turface (Turface Athletics) in a 1:1 mixture. Plants were grown under nitrogen-free conditions in a growth chamber programmed for 16-h light at 22 °C and 8-h dark at 20 °C. For nodulation assay, roots of one-wk-old seedlings were flood-inoculated with rhizobial bacteria, with each plant receiving ~1.0 mL cell suspension with an optical density of $OD_{600} = 0.1$. Nodulation phenotypes were recorded 3 wk post inoculation.

Rhizobial Strains and Growth Conditions. The wild-type bacterial strains used in this study are listed in *SI Appendix*, Table S2. The strains used for fluorescence microscopy contained either the plasmid pHC60 containing a constitutively expressed GFP or the plasmid pBHR-mRFP harboring a constitutively expressed red fluorescent protein. The mutant strains, including Rm41_*rns1*::Tn, Rm41Δ*tolC*, AK83Δ*rns1*, and Sm11Δ*rns1* were generated as described below. Strains were cultured on the TY agar medium at 28 °C with appropriate antibiotics.

Complementation Tests and CRISPR/Cas9-Mediated Gene Knockouts. For complementation tests, the genomic fragments of *Medtr8g028110* (*NS1a*) and *Medtr8g028115* (*NS1b*) were PCR-amplified from F83005 and cloned into the binary vector pCAMBIA1305.1 using the In-Fusion Advantage PCR Cloning Kits (Clontech). The expression of these genes was driven by their native promoters. The vector also contained a GUS reporter gene, allowing for identification of transgenic roots through GUS staining. The CRISPR/Cas9 gene knockout constructs were developed using the pKSE401 vector (46). Three pairs of oligos were designed to specifically target *NS1a, NS1b*, and both *NS1a* and *NS1b*, respectively (*SI Appendix*, Fig. S4). The oligo pairs were first annealed to produce a double-stranded fragment with 4-nt 5′ overhangs at both ends and then ligated into the BsaI-digested pKSE401 vector. We also PCR-amplified the GUS gene expression cassette from pCAMBIA1305.1 and cloned into the pKSE401 vector.

Hairy Root Transformation and Analysis of the Transformed Roots. Plasmids carrying various gene expression cassettes were transformed into the *Agrobacterium rhizogenes* strain ARqua1, and hairy root transformations were performed following the published procedures (47). Composite transgenic plants were transferred to plastic pots filled with a 1:1 mixture of sterilized vermiculite and turface and grown for 1 wk before inoculation. The transformed roots were distinguished from wild-type roots by GUS staining. For CRISPR/Cas9-based knockout experiments, transgenic roots were subjected to DNA isolation, PCR amplification, and DNA sequencing to validate the targeted DNA mutations. If the initial sequencing indicated the presence of multiple heterogeneous mutant alleles, the PCR products were ligated into the pGEM T-Easy Vector System (Promega), and 10 to 15 colonies were selected for sequencing.

Promoter Activity Analysis. Putative promoter regions of *NS1a* (1,152 bp) and *NS1b* (2,029 bp) were PCR-amplified from the genomic DNA of F83005 using primers containing the *attB* sites. The fragments were first cloned into the entry vector pDONR/Zeo (Invitrogen) and then subcloned into the destination vector pMDC163 carrying a GUS reporter gene to create promoter-GUS constructs using the Gateway cloning system (Invitrogen). The same promoters were also used to drive an eYFP reporter fused with a NLS at the C terminus. For this purpose, the *GUS* gene in the promoter-GUS constructs was replaced with the eYFP-NLS fusion. The e*YFP-NLS* fragment was amplified from the pSITE-3CA vector (48) with the primer pair containing the Xba I and Sac I restriction sites and a C-terminal nuclear localization signal. The plasmids carrying these promoter fusions were transformed into the *A. rhizogenes* strain ARqua1 for hairy root transformation.

Subcellular Localization and BiFC Assay. The full-length cDNA of *NS1a* and an alternatively spliced cDNA lacking the kinase domain coding sequence of *NS1b* were cloned into the entry vector pDONR/ZEO (Invitrogen) through the Gateway BP reaction (Invitrogen). For subcellular localization, the fragments were recombined into the pSITE_2NB vector (47) with an eGFP reporter fused at their C-termini under control of a double 35S promoter. As a control, we used the pCMU-PMr vector expressing AtPIP2a-mCherry under control of the AtUBQ10 promoter as a plasma membrane marker (49). For BiFC, the *NS1a* and *NS1b* fragments were recombined into the pSITE-nYFP-N1 and pSITE-cYFP-N1 vectors (48), respectively. We also cloned the *Medicago DMI2* gene into the same vectors to test its association with NS1a and NS1b. These plasmids were transformed into *Agrobacterium tumefaciens* strain LBA4404. For agroinfiltration in *Nicotiana benthamiana*, the *Agrobacterium* strains carrying different expression constructs were grown overnight in a liquid Luria-Bertani (LB) medium supplemented with appropriate antibiotics. Cells were harvested by centrifugation and resuspended in infiltration buffer containing 10 mM $MgSO_4 \cdot 7H_2O$ and 100 μM acetosyringone. Leaves of 3 to 4-wk-old *N. benthamiana* plants were infiltrated with needleless syringes. For subcellular localization, the diluted bacterial culture ($OD_{600} = 0.2$) was mixed with a 1/10 volume of an *A. tumefaciens* strain expressing the silencing suppressor p19. For BIFC, *N. benthamiana* leaves were coinfiltrated with 10:10:1 v/v mixture strains expressing tested pairs of pSITE-nYFP-N1, pSITE-cYFP-N1 fusions, and p19, respectively. Infiltrated plants were grown under normal growth conditions for 48 to 72 h. Fluorescence imaging was performed using an Olympus Fluoview FV1000 confocal microscope

Expression and Purification of the Ectodomains of NS1a, NS1b, and DMI2. We used Simple Modular Architecture Research Tool (SMART) (https://smart.embl.de) to predict the SP, ECD, and TM of the receptor-like kinases (50). The ECD coding sequences (excluding the signal sequences) were codon-optimized and fused in frame with an N-terminal gp67 secretion SP and a C-terminal hexahistidine (HIS) or FLAG tag for insect cell expression (GeneScript). These fragments were cloned into the transfer vector pFastBac1, and recombinant baculoviruses were obtained using the Bac-to-Bac Baculovirus Expression System following the protocols provided by the manufacturer (Thermo Scientific). Briefly, the pFastBac1 constructs were transformed into DH10Bac competent cells for site-specific transposition of the expression cassette into bacmid. Purified bacmid DNA was then transfected into Sf9 insect cells using Cellfectin II and cultured at 26 °C in the Sf-900 II SFM medium. After three rounds of virus amplification, fresh Sf9 cells were infected with recombinant passage-three virus particles (1:100 volume ratio to Sf-900 II SFM medium) and cultured in suspension for 4 d. Medium supernatant was harvested by centrifugation and was subjected to protein purification. Purification of HIS-tagged proteins was performed using the HisPur Ni-NTA Resin (Thermo Scientific) following the manufacturer's instructions. The FLAG-tagged proteins were purified with Pierce Anti-DYKDDDDK Magnetic Agarose (Thermo Scientific).

In Vitro Pull-Down Assay. A medium supernatant containing the insect cell-expressed FLAG-tagged ECD domain of NS1a ($NS1a^{ECD}$-FLAG) was added to the prewashed anti-FLAG magnetic agarose beads (Thermo Scientific) and incubated at 4 °C with mixing for 30 min. The beads were then magnetically harvested and washed three times with a washing buffer (phosphate-buffered saline, PH 7.4) and one time with purified water. The beads bound by $NS1a^{ECD}$-FLAG were

subsequently mixed with the purified HIS-tagged ECD domain of NS1a (NS1a^{ECD}-HIS), NS1b (NS1b^{ECD}-HIS), or DMI2 (DMI2^{ECD}-HIS) and incubated at 4 °C for 3 h with gentle shaking in a binding buffer (25 mM TrisHCl pH 7.4, 150 mM NaCl, 1% NP-40, 1 mM EDTA, 5% glycerol). The magnetic agarose beads were then collected with a magnetic stand and washed three times with a washing buffer. The pull-down proteins were eluted by an elution buffer (Pierce™ 3× DYKDDDDK Peptide) and detected by an immunoblot with an anti-HIS antibody.

Random Transposon Insertion Mutagenesis of Rm41 and Screen of Mutants that Altered the Nodulation Phenotype. The mariner transposon pSAM_RI vector (36) was introduced into an Rm41 derivative resistant to streptomycin by biparental mating. The donor *E. coli* strain WM3064 carrying the transposon vector and the recipient strain Rm41 were cultured in the LB medium supplemented with 0.3 mM diaminopimelic acid (LB DAP) or with 1 mM $MgSO_4$ and 1 mM $CaCl_2$ (LB MC), respectively, to an OD_{600} of ~1.2 to 1.5 and were pooled in a ratio of 1.0 mL recipient to 0.5 mL donor in a 1.5-mL Eppendorf tube. After centrifugation at 12,500 rpm for 3 min, the pellet was washed and then suspended in 100 μL sterile distilled water. The cell suspension was then spotted onto a LB MC DAP agar plate and incubated overnight at 30 °C. The conjugation spot was scraped and suspended in 1.0 mL sterile distilled water, and 100 μL of the suspension was spread onto a LB MC agar plate supplemented with 400 μg/mL kanamycin and 100 μg/mL streptomycin and incubated at 30 °C for 3 d. Rhizobial conjugants resistant to kanamycin and streptomycin were washed down with the liquid LB medium containing 20% (v/v) glycerol and stored at −80 °C until further use.

The mutant libraries were inoculated onto the roots of F83005 seedlings. Nodules induced by the mutants were collected, surface sterilized with 70% (v/v) ethanol for 3 min, washed in a large volume of sterile distilled water, and then crushed in 200 μL water. A dilution series of the suspensions were spread onto LB MC plates with 200 μg/mL kanamycin and 100 μg/mL streptomycin. Genomic DNA samples were isolated from the colonies, digested with XbaI and EcoRI enzymes, and the fragments were ligated into the pBluescript vector. After transformation of the ligated DNA into *E. coli* MDS42 RecA blue cells (Scarab Genomics Inc.), colonies resistant to both ampicillin and kanamycin were isolated. Sequences flanking the transposon insertion sites were determined with the help of the transposon-specific primers.

Site-Directed Mutagenesis of Rm41. For plasmid integration mutagenesis, internal fragments of the targeted genes were amplified and cloned into the pK19mob vector. For resistance cassette mutagenesis, ~1.5 to 2.0-kb targeted gene fragments were first amplified and cloned into pK18mobSacB, and then a spectinomycin resistance cassette was amplified and cloned into the middle of the gene fragments in the vector. For targeted gene deletions, DNA fragments of similar size upstream and downstream of the targeted deletion were joined and cloned into vector pK18mobSacB. The constructs were introduced into rhizobia by biparental mating as described above, and bacteria with the construct integrated into the bacterial genome via homologous recombination were selected on a medium containing kanamycin (400 μg/mL). For the isolation of mutants with the insertion of the antibiotic cassette or with deletion, single colonies were chosen randomly and inoculated into 1.0 mL liquid LB MC medium. After 12 to 16-h inoculation, 100 μL from serial dilutions were spread on LB MC plates containing 10% sucrose. Single colonies that appeared on the sucrose-containing plates were replicated on LB MC (and 100 μg/mL spectinomycin in the case of the cassette insertion mutants) and LB MC with 200 μg/mL kanamycin. Kanamycin-sensitive colonies that lost the vector via recombination through the second flanking fragment were tested by colony PCR for the presence of the deletion or the antibiotic cassette insertion.

Assay for Rns1 Secretion. To test the secretion of Rns1, a pHC60 plasmid expressing both an HA-tagged Rns1 and a GFP protein was transformed into Rm41_*rns1*::Tn and Rm41Δ*tolC*. Bacterial cultures were grown overnight at 28 °C in a TY medium to an optical density of OD_{600} = 0.5–0.6. The bacterial cells and supernatants were harvested by centrifugation for 15 min at 10,000 rpm at 4 °C. The cell pellets were resuspended in an 1× PBS buffer supplemented with 10 mM β-mercaptoethanol and sonicated for 12 s for 10 times at 4 °C to yield a preparation of total cellular proteins. Supernatant proteins were concentrated by precipitation with 20% trichloroacetic acid (w/v) and incubated on ice for at least 1 h, followed by centrifugation at 4,000 rpm for 20 min at 4 °C. The protein pellets were washed three times with 0.01M HCl/90% acetone. Cellular and supernatant proteins from an equivalent of 10 mL cell culture were separated by sodium dodecyl sulfate-polyacrylamide gel electrophoresis with 12.5% acrylamide and visualized by an immunoblot with an anti-HA or anti-GFP antibody. The gel band detected by anti-HA antibody was subjected to liquid chromatography with tandem mass spectrometry after trypsin digestion, using the services provided by MS Bioworks.

Data, Materials, and Software Availability. All study data are included in the article and/or *SI Appendix*. The sequences reported in this paper have been deposited in the GenBank database (accession nos. OP846969 and OP846970).

ACKNOWLEDGMENTS. We thank E. Kondorosi for helpful comments on the manuscript; and P. Tiffin (University of Minnesota), B. Scharf (Virginia Polytechnic Institute and State University), and A. Mengoni (University of Florence, Italy) for providing the rhizobial strains. This work was supported by US Department of Agriculture/National Institute of Food and Agriculture Grant 2014-67013-21573 (to H.Z.), US National Science Foundation Grant IOS-1758037 (to H.Z. and A.M.), US Department of Agriculture/Agricultural Research Service Non-Assistance Cooperative Agreement Grant 5850428003 (to H.Z.), Hungarian National Research, Development and Innovation Office Grants K128486 and K134841 (to A. Kereszt), and China Scholarship Council (to T.W.).

Author affiliations: [a]Department of Plant and Soil Sciences, University of Kentucky, Lexington, KY 40546; [b]Institute of Plant Biology, Biological Research Centre, Szeged 6726, Hungary; [c]Cereals Crops Research Unit, U.S. Department of Agriculture, Agricultural Research Service, Fargo, ND 58102; [d]Forage-Animal Production Research Unit, U.S. Department of Agriculture, Agricultural Research Service, Lexington, KY 40546; [e]Department of Genetics and Molecular Biology, University of Pécs, Pécs H-7604, Hungary; [f]Complex Carbohydrate Research Center, University of Georgia, Athens, GA 30602; and [g]Department of Microbiology and Molecular Biology, Brigham Young University, Provo, UT 84602

1. D. Couto, C. Zipfel, Regulation of pattern recognition receptor signalling in plants. *Nat. Rev. Immunol.* **16**, 537–552 (2016).
2. J. D. Jones, R. E. Vance, J. L. Dangl, Intracellular innate immune surveillance devices in plants and animals. *Science* **354**, aaf6395 (2016).
3. C. Zipfel, G. E. Oldroyd, Plant signalling in symbiosis and immunity. *Nature* **543**, 328–336 (2017).
4. T. Nakagawa *et al.*, From defense to symbiosis: Limited alterations in the kinase domain of LysM receptor-like kinases are crucial for evolution of legume-*Rhizobium* symbiosis. *Plant J.* **65**, 169–180 (2011).
5. M. Lopez-Gomez, N. Sandal, J. Stougaard, T. Boller, Interplay of flg22-induced defence responses and nodulation in *Lotus japonicus*. *J. Exp. Bot.* **63**, 393–401 (2012).
6. K. Miyata *et al.*, The bifunctional plant receptor, OsCERK1, regulates both chitin-triggered immunity and arbuscular mycorrhizal symbiosis in rice. *Plant Cell Physiol.* **55**, 1864–1872 (2014).
7. E. Limpens, A. van Zeijl, R. Geurts, Lipochitooligosaccharides modulate plant host immunity to enable endosymbioses. *Annu. Rev. Phytopathol.* **53**, 311–334 (2015).
8. Z. Bozsoki *et al.*, Receptor-mediated chitin perception in legume roots is functionally separable from Nod factor perception. *Proc. Natl. Acad. Sci. U.S.A.* **114**, E8118–E8127 (2017).
9. Z. Bozsoki *et al.*, Ligand-recognizing motifs in plant LysM receptors are major determinants of specificity. *Science* **369**, 663–670 (2020).
10. S. Pfeilmeier *et al.*, Expression of the *Arabidopsis thaliana* immune receptor EFR in *Medicago truncatula* reduces infection by a root pathogenic bacterium, but not nitrogen-fixing rhizobial symbiosis. *Plant Biotechnol J.* **17**, 569–579 (2019).
11. D. Wang, S. Yang, F. Tang, H. Zhu, Symbiosis specificity in the legume-rhizobial mutualism. *Cell Microbiol.* **14**, 334–342 (2012).
12. T. Rey, A. Chatterjee, M. Buttay, J. Toulotte, S. Schornack, *Medicago truncatula* symbiosis mutants affected in the interaction with a biotrophic root pathogen. *New Phytol.* **206**, 497–500 (2015).
13. D. E. Cook, C. H. Mesarich, B. P. Thomma, Understanding plant immunity as a surveillance system to detect invasion. *Annu. Rev. Phytopathol.* **53**, 541–563 (2015).
14. G. E. Oldroyd, J. D. Murray, P. S. Poole, J. A. Downie, The rules of engagement in the legume-rhizobial symbiosis. *Annu. Rev. Genet.* **45**, 119–144 (2011).
15. J. L. Firmin, K. E. Wilson, R. W. Carlson, A. E. Davies, J. A. Downie, Resistance to nodulation of cv. Afghanistan peas is overcome by nodX, which mediates an O-acetylation of the *Rhizobium leguminosarum* lipo-oligosaccharide nodulation factor. *Mol. Microbiol.* **10**, 351–360 (1993).
16. G. V. Bloemberg *et al.*, A central domain of *Rhizobium* NodE protein mediates host specificity by determining the hydrophobicity of fatty acyl moieties of nodulation factors. *Mol. Microbiol.* **16**, 1123–1136 (1995).
17. S. Radutoiu *et al.*, LysM domains mediate lipochitin-oligosaccharide recognition and *Nfr* genes extend the symbiotic host range. *EMBO J.* **17**, 3923–3935 (2007).
18. R. Li *et al.*, Natural variation in host-specific nodulation of pea is associated with a haplotype of the SYM37 LysM-type receptor-like kinase. *Mol. Plant. Microbe Interact.* **24**, 1396–1403 (2011).
19. N. Fraysse, F. Couderc, V. Poinsot, Surface polysaccharide involvement in establishing the rhizobium-legume symbiosis. *Eur. J. Biochem.* **270**, 1365–1380 (2003).

20. W. J. Deakin, W. J. Broughton, Symbiotic use of pathogenic strategies: Rhizobial protein secretion systems. *Nat. Rev. Microbiol.* **7**, 312–320 (2009).
21. Y. Kawaharada *et al.*, Receptor-mediated exopolysaccharide perception controls bacterial infection. *Nature* **523**, 308–312 (2015).
22. S. Yang, F. Tang, M. Gao, H. B. Krishnan, H. Zhu, R gene-controlled host specificity in the legume-rhizobia symbiosis. *Proc. Natl. Acad. Sci. U.S.A.* **107**, 18735–18740 (2010).
23. M. Sugawara *et al.*, Variation in bradyrhizobial NopP effector determines symbiotic incompatibility with *Rj2*-soybeans via effector-triggered immunity. *Nat. Commun.* **9**, 3139 (2018).
24. S. Okazaki, T. Kaneko, S. Sato, K. Saeki, Hijacking of leguminous nodulation signaling by the rhizobial type III secretion system. *Proc. Natl. Acad. Sci. U.S.A.* **110**, 17131–17136 (2013).
25. A. Teulet *et al.*, The rhizobial type III effector ErnA confers the ability to form nodules in legumes. *Proc. Natl. Acad. Sci. U.S.A.* **116**, 21758–21768 (2019).
26. F. Tang, S. Yang, J. Liu, H. Zhu, *Rj4*, a gene controlling nodulation specificity in soybeans, encodes a thaumatin-like protein but not the one previously reported. *Plant Physiol.* **170**, 26–32 (2016).
27. B. Zhang *et al.*, *Glycine max NNL1* restricts symbiotic compatibility with widely distributed bradyrhizobia via root hair infection. *Nat. Plants.* **7**, 73–86 (2021).
28. M. Yasuda *et al.*, Effector-triggered immunity determines host genotype-specific incompatibility in legume-*Rhizobium* symbiosis. *Plant Cell Physiol.* **57**, 1791–1800 (2016).
29. J. Liu, S. Yang, Q. Zheng, H. Zhu, Identification of a dominant gene in *Medicago truncatula* that restricts nodulation by *Sinorhizobium meliloti* strain Rm41. *BMC Plant Biol.* **14**, 167 (2014).
30. S. Weidner *et al.*, Genome Sequence of *Sinorhizobium meliloti* Rm41. *Genome Announc.* **1**, e00013–12 (2013).
31. N. Young *et al.*, The *Medicago* genome provides insight into the evolution of rhizobial symbioses. *Nature* **480**, 520–524 (2011).
32. K. Schiessl *et al.*, Nodule inception recruits the lateral root developmental program for symbiotic nodule organogenesis in *Medicago truncatula*. *Curr. Biol.* **29**, 3657–3668.e5 (2019).
33. S. Carrere, S. J. Verdier, P. Gamas, MtExpress, a comprehensive and curated RNAseq-based gene expression Atlas for the model legume Medicago truncatula. *Plant Cell Physiol.* **62**, 1494–1500 (2021).
34. B. Roux *et al.*, An integrated analysis of plant and bacterial gene expression in symbiotic root nodules using laser-capture microdissection coupled to RNA sequencing. *Plant J.* **77**, 817–837 (2014).
35. E. Larrainzar *et al.*, Deep sequencing of the *Medicago truncatula* root transcriptome reveals a massive and early interaction between nodulation factor and ethylene signals. *Plant Physiol.* **169**, 233–265 (2015).
36. B. J. Perry, C. K. Yost, Construction of a mariner-based transposon vector for use in insertion sequence mutagenesis in selected members of the *Rhizobiaceae*. *BMC Microbiol.* **14**, 298 (2014).
37. M. D. Yoder, N. T. Keen, F. Jurnak, New domain motif: The structure of pectate lyase C, a secreted plant virulence factor. *Science* **260**, 1503–1507 (1993).
38. C. Finnie, A. Zorreguieta, N. M. Hartley, J. A. Downie, Characterization of *Rhizobium leguminosarum* exopolysaccharide glycanases that are secreted via a type I exporter and have a novel heptapeptide repeat motif. *J. Bacteriol.* **180**, 1691–1699 (1998).
39. S. Schneiker-Bekel *et al.*, The complete genome sequence of the dominant *Sinorhizobium meliloti* field isolate Sm11 extends the *S. meliloti* pan-genome. *J. Biotechnol.* **155**, 20–33 (2011).
40. M. Galardini *et al.*, Exploring the symbiotic pangenome of the nitrogen-fixing bacterium *Sinorhizobium meliloti*. *BMC Genomics.* **12**, 235 (2011).
41. A. M. Cosme *et al.*, The outer membrane protein TolC from *Sinorhizobium meliloti* affects protein secretion, polysaccharide biosynthesis, antimicrobial resistance, and symbiosis. *Mol. Plant Microbe Interact.* **21**, 947–957 (2008).
42. A. Becker, N. Fraysse, L. Sharypova, Recent advances in studies on structure and symbiosis-related function of rhizobial K-antigens and lipopolysaccharides. *Mol. Plant Microbe Interact.* **18**, 899–905 (2005).
43. K. M. Jones, H. Kobayashi, B. W. Davies, M. E. Taga, G. C. Walker, How rhizobial symbionts invade plants: The *Sinorhizobium-Medicago* model. *Nature Rev. Microbiol.* **5**, 619–633 (2007).
44. J. A. Downie, The roles of extracellular proteins, polysaccharides and signals in the interactions of rhizobia with legume roots. *FEMS Microbiol. Rev.* **34**, 150–170 (2010).
45. A. Silipo *et al.*, Glyco-conjugates as elicitors or suppressors of plant innate immunity. *Glycobiology* **20**, 406–419 (2010).
46. H. L. Xing *et al.*, A CRISPR/Cas9 toolkit for multiplex genome editing in plants. *BMC Plant Biol.* **14**, 327 (2014).
47. A. Boisson-Dernier *et al.*, *Agrobacterium rhizogenes*-transformed roots of *Medicago truncatula* for the study of nitrogen-fixing and endomycorrhizal symbiotic associations. *Mol. Plant Microbe Interact.* **14**, 695–700 (2001).
48. R. Chakrabarty *et al.*, PSITE vectors for stable integration or transient expression of autofluorescent protein fusions in plants: Probing *Nicotiana benthamiana*-virus interactions. *Mol. Plant Microbe Interact.* **20**, 740–750 (2007).
49. S. Ivanov, M. J. Harrison, A set of fluorescent protein-based markers expressed from constitutive and arbuscular mycorrhiza-inducible promoters to label organelles, membranes and cytoskeletal elements in *Medicago truncatula*. *Plant J.* **80**, 1151–1163 (2014).
50. I. Letunic, S. Khedkar, P. Bork, SMART: Recent updates, new developments and status in 2020. *Nucleic Acids Res.* **49**, D458–D460 (2021).